Research Square

Preprints are preliminary reports that have not undergone peer review.
They should not be considered conclusive, used to inform clinical practice,
or referenced by the media as validated information.

Advanced Catalysts for Renewable Biofuel Production: Co-Pyrolysis of EFB and UCO over Transition Metal–Doped Cerium/Eggshell-Derived CaO

Yaw Huei Yat
University of Technology Malaysia
Vekes Balasundram
vekes@utm.my

University of Technology Malaysia
Norazana Ibrahim
University of Technology Malaysia
Ruzinah Isha
Universiti Malaysia Pahang Al-Sultan Abdullah, Lebuh Persiaran Tun Khalil Yaakob
Le Kim Hoang Pham
Nguyen Tat Thanh University, Viet Nam
Suan Shi
China Agricultural University

Article

Keywords: Biomass, Cooking oil, Eggshell, Pyrolysis, Biofuel, Hydrocarbons

Posted Date: May 26th, 2026

DOI: https://doi.org/10.21203/rs.3.rs-9618869/v1

License: This work is licensed under a Creative Commons Attribution 4.0 International License.
Read Full License

Additional Declarations: No competing interests reported.

Abstract

In Malaysia, empty fruit bunch (EFB) is a potential biomass for biofuel production via pyrolysis. However, EFB generates biofuel rich in oxygenated compounds. Used cooking oil (UCO) is generated as waste by the food industry and is primarily disposed of in the environment. UCO is composed mainly of fatty acids, which can act as hydrocarbon enhancers during pyrolysis. Commercial zeolites used as catalysts in pyrolysis suffer from rapid coking, easy deactivation, high acidity, and poor environmental friendliness. Chicken eggshells are rich in calcium oxide (CaO), which can act as an alkaline support and an environmentally friendly catalyst. Hence, to our knowledge, no studies have focused on co-pyrolyzing EFB with UCO over an eggshell-derived CaO (CaO-Ces) catalyst to produce biofuel. Therefore, this study aims to evaluate the physicochemical properties of various bimetallic (Ni-Ce, Fe-Ce, Mn-Ce, Co-Ce, Cu-Ce, and Zn-Ce) modified CaO-Ces and examine their catalytic performance in the co-pyrolysis of EFB and UCO. Bimetallic-modified CaO-Ces were prepared using the incipient wetness impregnation method and characterized for phase analysis, surface morphology, and textural properties. Pyrolysis was conducted at 500°C in a fixed-bed horizontal reactor, with oil product analysis performed using gas chromatography/mass spectrometry (GC/MS). For comparison, the non-catalytic, eggshell-derived CaO (CaO-Ces), and Ce/CaO-ces catalysts were also pyrolysed under the same conditions. The results indicate that the highest pyrolysis oil was achieved by Mn-Ce/CaO-Ces (73.03%), followed by Cu-Ce/CaO-Ces (66.05%), Co-Ce/CaO-Ces (60.87%), Zn-Ce/CaO-Ces (60.73%), Ni-Ce/CaO-Ces (59.30%), Fe-Ce/CaO-Ces (58.75%), Ce/CaO-Ces (53.69%), and CaO-Ces (30.09%). For the hydrocarbons yield, Zn-Ce/CaO-Ces has the highest at 39.53%. These findings suggest that Zn-Ce/CaO-Ces represent a viable and sustainable alternative to conventional catalysts, offering high efficiency and environmental compatibility for converting biomass and cooking oil waste into fuel.

1. Introduction

As one of the world's leading oil and gas producers, Malaysia is addressing the transition to renewable energy by adopting various energy sources to reduce greenhouse gas (GHG) emissions by up to 70% by 2050. However, conventional fossil fuels continue to play a crucial role as the primary energy source. The implementation of biomass energy, along with potential barriers for infrastructure and initiatives to utilise organic waste components, is promising and warrants further, detailed exploration. Referencing the Global Waste Management Outlook 2024 released by the United Nations Environment Programme on 28 February 2024, the total waste expected to be collected by 2050 is 3.40 tonnes, 1.7 times higher than the 2.01 tonnes produced in 2023, with rich natural resources and studies on biomass demonstrating that biomass energy is a promising feedstock for Malaysia to achieve its target of transforming the land into a 70% carbon-free country by 2050 [1]. As the world’s second-largest exporter of oil palm, Malaysia has numerous opportunities to test and develop new approaches to reduce its carbon footprint by substituting energy resources and fuels for automobiles and other transportation modes. The exploitation of palm biodiesel is projected to reach approximately 0.4 million tonnes by 2035.

In Malaysia, it is estimated that during the palm oil milling process, about 230 to 250 kg of palm biomass, such as empty fruit bunch (EFB), is produced per tonne of raw fruit, in addition to oil palm fronds (OPF) and palm kernel shells (PKS) [2]. Domestic demand for continuous biofuel supply increased to 529,000 tonnes in October 2019. The use of biomass, such as EFB, offers a range of advantages that benefit not only the economy but also the environment and society, providing benefits superior to those from petroleum and other renewable energy sources.

Thermochemical and biological treatments are the two primary technologies commonly used to produce renewable fuel energy from naturally occurring organic compounds. Thermochemical treatment can be categorised into three methods: pyrolysis, gasification, and torrefaction. For converting biomass into biofuel at standard atmospheric pressure (1 atm), many researchers agree that pyrolysis is the most effective and sustainable approach for managing the disposal of excess biomass, while also reducing the operational costs of pyrolysis equipment and electricity [3]. Pyrolysis is recommended because it offers several advantages, including the production of various oxygenated compounds, such as carboxylic acids, aldehydes, and lignin-derived oligomers, as well as hydrocarbons. When feedstocks with most of their moisture removed are thermally decomposed at elevated temperatures, especially under an inert atmosphere (such as nitrogen, helium, or argon), the process completes more quickly. Biomasses chosen for previous studies on pyrolysis include rice husk ash, pineapple peels, corncobs, and wheat straw. However, the high viscosity and acidity, accompanied by low heating values, built up a boundary.

To overcome these issues, the introduction of co-pyrolysis, by using two or more biomass feedstocks in the same reactor, offers improved stability and higher heating value (> 28 MJ/kg). Industries commonly utilize empty fruit bunches (EFB) from oil palm residues to produce pyrolysis oil due to their high content of lignocellulosic components, which include cellulose, hemicellulose, and lignin. In our previous work [3], we conducted a co-pyrolysis study of EFB and UCO and found that UCO served as a hydrocarbon enhancer during co-pyrolysis with EFB. The addition of UCO increased the hydrocarbons from 45.5 to 63.7 wt.% compared to the pyrolysis of EFB, which had 0 wt.% of hydrocarbons.

In a previous study [3], Hydrogen-based Zeolite Socony Mobil-5 (HZSM-5), a catalyst frequently used in catalytic pyrolysis, was doped with transition metals, including nickel (Ni) and molybdenum (Mo), to enhance the catalytic cracking of hydrocarbons. Although HZSM-5 is widely applied in industrial-scale catalytic pyrolysis, it has numerous drawbacks, including deactivation, rapid coking, and environmental concerns. To add to the existing limitation, high expenses also arose from the purchase of HZSM-5. To address all potential issues as mentioned, a new green catalyst should be developed. Additionally, the food waste issues faced by Malaysians nowadays, especially with egg consumption, are a significant concern, as they are a necessary part of daily needs, leading to the massive generation of chicken eggshells (Ces) upon consumption. Emissions of hazardous particles and compounds, such as hydrogen sulphide (H_2S) and certain unpleasant odours, attract pests, promote the growth of harmful bacteria, and pollute water resources, soil, and the environment. Improper disposal of Ces has raised concerns across various industries, with an estimated 7.83–10.44 million tonnes generated in recent

years. Given its carbonaceous composition, it is summarized that the $CaCO_3$ content can be a good indicator for producing fertilizers and other supplements, biodiesel catalysts, clay bricks, and thermal insulating materials [4]. As chicken eggshells are in the solid phase, catalytic pyrolysis is usually carried out using a heterogeneous catalyst in-situ [5]. The eggshells disposed of daily can be converted into a calcium oxide-based catalyst for use in the transesterification process and, to a limited extent, in the pyrolysis process. Alkaline catalysts are preferred by many industry players because they offer promising recyclability and facilitate easier separation. Due to its high alkalinity, the eggshell-based CaO catalyst has been shown to be a more effective medium for minimizing coking [6].

Another limitation that affects the hydrocarbons in pyrolysis oil is the presence of oxygenated compounds. The oxygen remaining in the oil will form other side components, including alcohols, esters, ketones, aldehydes, and phenols. To reduce the formation of oxygenated compounds, the addition of cerium oxide (CeO_2) may overcome this dilemma, as it exhibits catalytic properties that help avoid structural defects and high reactive oxygen species [7]. The addition of cerium can be achieved through doping.

Hence, this study investigates the effect of a CaO-ces catalyst loaded with cerium oxides and modified with nickel (Ni), manganese (Mn), iron (Fe), copper (Cu), cobalt (Co), and zinc (Zn) on the co-pyrolysis of EFB and UCO. UCO was selected due to its wide availability from households nationwide and based on its favourable physicochemical properties. The catalytic performance of Ce/CaO-ces was evaluated in terms of pyrolysis oil yields and hydrocarbon selectivity, aligned with the primary goals, which are to address drawbacks of conventional catalysts and the lack of comprehensive studies on the metallic modified eggshell-based catalysts for oil palm-based biomass pyrolysis, with the hydrocarbon conversion from used cooking oil.

2. Methodology

2.1. Catalyst Preparation

In this study, calcium oxide (CaO) derived from waste chicken eggshells was used as the catalyst's support, which was labelled as CaO-ces. The preparation method for this support is described in our previous work [6]. Next, the incipient wetness impregnation (IWI) method was used to develop bimetallic modified CaO-ces catalysts. First, metal salts such as cerium (III) nitrate hexahydrate ($Ce(NO_3)_3{\cdot}6H_2O$, 99% purity), zinc nitrate hexahydrate ($Zn(NO_3)_2{\cdot}6H_2O$, 98% purity), iron (III) nitrate nonahydrate ($Fe(NO_3)_3{\cdot}9H_2O$, 99% purity), nickel (II) nitrate hexahydrate ($Ni(NO_3)_2{\cdot}6H_2O$, 99% purity), manganese (II) nitrate tetrahydrate ($Mn(NO_3)_2{\cdot}4H_2O$, 98% purity), copper (II) nitrate trihydrate ($Cu(NO_3)_2{\cdot}3H_2O$), and cobalt(II) nitrate hexahydrate ($Co(NO_3)_2{\cdot}6H_2O$, 99% purity) were purchased from ACROS Organics. Next, 1 wt.% cerium salts, 1 wt.% zinc salts, 98 wt.% CaO-ces, and 80 mL of deionized water were mixed in a beaker. Then, the mixture was transferred to a hot plate magnetic stirrer and stirred thoroughly for 4 hours at 80°C. Afterwards, the mixture was dried in a microwave oven at 105°C until the weight remained

constant, to remove moisture. Finally, the dried solid was transferred to a muffle furnace and calcined at 600°C for 3 hours to thermally stabilise the catalyst and promote fusion between the metal oxides and CaO-ces, thereby preventing further degradation during pyrolysis. The resulting catalyst was collected, sieved to 50 microns, and labelled as Zn-Ce/CaO-ces. Similar IWI methods were applied to produce other bimetallic modified CaO-ces catalysts, such as Fe-Ce/CaO-ces, Ni-Ce/CaO-ces, Mn-Ce/CaO-ces, Cu-Ce/CaO-ces, and Co-Ce/CaO-ces. Meanwhile, Ce/CaO-ces was developed with a fixed cerium content of 1 wt.% as the benchmark catalyst. All the synthesized catalysts were characterized for their physicochemical properties, such as phase analysis, surface morphology, and textural properties (surface area, total pore volume, and average pore diameter). The detailed steps of characterization techniques can be found in our previous work [8].

2.2. Catalytic pyrolysis

The effects of bimetallic-modified CaO-ces catalysts on the pyrolysis of EFB and UCO were evaluated using a laboratory-scale fixed-bed reactor (Fig. 2.1). The experimental setup included a tubular furnace for heating, a condenser system, a gas collection bag, and a nitrogen (N_2) supply. EFB was purchased from a local palm mill company in Selangor, Malaysia, and its preparation method is described in our previous work [9]. Next, UCO was collected from nearby restaurants in the Kuala Lumpur area, and the preparation method for UCO is described in our previous work [10]. Before the pyrolysis experiment, 4 g of the mixed EFB and UCO at a fixed mass loading ratio of 1:1 was blended, and 4 g of synthesized catalyst was kept separate using a stainless steel 400 mesh to facilitate catalyst recovery and ensure vapours pass through the catalyst. Both were placed in the fixed-bed reactor, maintaining a catalyst-to-feedstock mass ratio of 1:1. All input and output connections were tightened securely to prevent leakage. Nitrogen (N_2) gas was used to purge the reactor to ensure an inert, nonreactive environment at a flow rate of 80 mL/min. The experiments were conducted under atmospheric pressure (1 atm).

In the experiment, the temperature remained constant as the tubular furnace was heated to the target reaction temperature of 500°C. The pyrolysis process was carried out for one hour, including cooling time. As the pyrolysis reaction proceeded, the resulting volatile compounds were carried by the N_2 stream out of the reactor and directed into a condenser system, where a filtering flask immersed in room temperature water (maintained at 25°C) condensed the vapours. The gaseous products were condensed into pyrolysis oil, which was collected and analysed for chemical composition by gas chromatography/mass spectrometry (GC/MS; Agilent, G3171A). The standard operating procedures for GC/MS analysis were reported in our previous work [8]. Meanwhile, microparticles and non-condensable gases were captured in a gas bag. After each experiment, the reactor was disassembled and cooled to room temperature. The residual solid materials were then recovered and weighed.

3. Results and Discussions

3.1. Phase analysis

The phase purity and crystallinity of the ceria-treated, metallic-modified catalysts were measured through X-Ray diffraction (XRD). The XRD patterns obtained for chicken eggshell-based calcium oxide (CaO-ces), ceria-treated CaO-ces, and metallic modified catalysts using nickel (Ni), zinc (Zn), manganese (Mn), iron (Fe), copper (Cu), and cobalt (Co) were summarized into a line chart as shown in Fig. 3.1. Based on Fig. 3.1, XRD patterns of CaO-ces and Ce/CaO-ces possess the same peak occurring at 32.54° and 53.10°. Similar to a study carried out on degrading anthracene/fluorene using cerium oxide particles [11], which the peaks were formed at several degrees, including degrees around 32.54° and 53.10° respectively. The XRD patterns were observed at angles ranging from 5° to 100°. Based on Fig. 3.1 compared to CaO-ces, eight peaks were observed at the Ce/CaO-ces pattern, which emerged at the degrees, 2θ of 19.07°, 27.67°, 34.02°, 48.21°, 51.08°, 64.26°, 73.19°, and 85.65°. Moreover, surprisingly, the peak emerged at 37.88° and disappeared after the addition of cerium oxide (Ce_2O_3). This could be due to the calcination temperature, which plays a key role in determining the catalyst's molecular structure. In a study on the effects of calcination temperature on phase composition, it was found that calcination temperatures above 500°C caused the peaks detected by XRD to become gradually sharper and narrower. It was believed that the temperature applied to the metal oxide caused the characteristic peak between 30° and 40° to flatten. It was found that the crystallite size increased due to the high temperature used during calcination [12]. Therefore, it is believed that the 650°C calcination temperature in this experiment converted the brookite phase of the Ce/CaO-Ce catalyst to anatase. The phase transformation occurs as the calcination temperature increases.

Another notable change in the XRD pattern shown in Fig. 3.1 that could be observed was located at the pattern of Ce/CaO-ces modified using nickel oxide (NiO). Additional peaks appeared at a 2θ equivalent to 68.45° and 92.38°, representing a small portion of nickel oxide (NiO) present on the surface of Ni-Ce/CaO-ces. The logical factor that drives peak formation at both significant degrees is the metal oxide loading. For details, Han et al. [13] mentioned that when there is more loading by metal oxide, a peak will be formed, signifying unequal nickel species aggregating on the catalyst's surface at different points. Therefore, Ni can promote stability through several methods, one of which involves controlling particle size, thereby forming tiny Ni crystallites. Interestingly, the distance between reactant particles can be reduced, resulting in lower resistance to the diffusion of ceria onto the CaO-ces and thereby increasing the frequency of reactant molecules adsorbing at active sites.

Another significant finding in Fig. 3.1 is that the peaks observed in Mn-Ce/CaO-ces were similar, with estimated 2θ values between 70° and 72.30°. Interestingly, the peaks for the Zn-modified catalyst mainly formed at 28°, 33°, 49°, and 57°, respectively, which align with the results obtained by Shah et al. [14]. The great dispersion of the peaks occurred due to the greater activity of manganese (Mn) compared to ceria. The utilization of Mn indirectly accelerates the washing rate, which, in turn, causes the crystalline size to decrease. Another reason that might be related to the different calcination temperatures. The heating inside the furnace would disrupt the catalytic structure, as the ions were activated and excited, causing dispersion; hence, the crystalline size decreased. For the calcination temperature applied to Mn-Ce/CaO-ces, set at 600°C, the 2θ values obtained are 28.6°, 33.0°, 47.5°, 56.4°, 59.3°, and 69.5°, respectively [6]. Two additional crystalline surfaces were discovered at degrees of 78.16° and 80.59°

from the CaO-ces catalyst doped with Zn. In pyrolysis oil produced using feedstock that underwent reaction with Fe-Ce/CaO-ces, a crystal-bound surface was observed at 2θ degrees of 72.30°, 78.16°, and 80.59°, indicating a combination of active surfaces at Mn-Ce/CaO-ces and Zn-Ce/CaO-ces, unlike Fe-modified Ce/CaO-ces. Those surfaces were completely dissolved in liquid hydrocarbons from the pyrolysis of the feedstock using Cu-Ce/CaO-ces. Meanwhile, for Co-Ce/CaO-ces, the only notable peak spotted was at a degree, 2θ of 80.59°. This indicates that neither Co nor Cu supported the expansion of the crystalline surface of Ce/CaO-ces. In a nutshell, a sufficient mass of redox-reaction-support catalyst and a favourable calcination temperature are crucial factors to be taken into account to ensure crystalline formation in a CaO-ces-based catalyst.

3.2. Surface morphology

Differences between the surface morphology of chicken eggshell-based calcium oxide (CaO-ces) treated and untreated using cerium (Ce) were observed using Field Emission Scanning Electrons Microscopy (FESEM). In our previous work [7], we found that the particles had similar longitudinal sizes and were evenly distributed (see FESEM Figs. 2(a) and 2(b)). There were a few agglomerated parts, believed to be clumps resulting from wet impregnation. The CaO-ces particles formed after calcination at a temperature of 900°C could be seen mainly comprising a cubical structure, with some empty spaces identified at the surface between the particles (Fig. 3.2). When the calcination temperature increases, the porosity of the CaO-ces catalyst decreases, as the initially densely packed structure causes the porous wall to collapse.

Similarly, Supriyanto et al. [15] reported that $CaCO_3$ experienced mass loss as CO_2 after calcination, making CaO-ces more porous than before calcination. To summarize the statement, the calcined CaO-ces was proved to be effective in eliminating any impurities that could affect the metal deposition on the surface of catalysts. For the surface morphology of cerium-treated CaO-ces (refer to Fig. 3.2 (a)), the shape of the catalyst was irregular and spherical. Without the addition of transition metals, many CaO catalysts did not have any tiny pores to allow EFB to attach onto and bind with the catalyst to carry out primary cracking. The changes in the Ce/CaO-ces shape can be potentially influenced by the transition metal's attachment on the surface and interacting with active sites or surface flaws of Ce-CaO catalysts. According to Windarti et al. [16], with the increase in cerium's charge, the interaction of cerium oxides with the chicken eggshell's surface became more frequent, as new surfaces formed resulted from chemical bonds breaking, creating a relaxed surface and reducing the band gap with the CaO-ces surface. Referring to the mechanical structure of the material surface treated using Ce, the big solid shape of Ce/CaO-ces represented a dumbbell-shaped morphology. This could be the outcome of electron transfer enhancement between the nanoparticles that do not appear in their individual counterparts. As a supporting information to support the statement, Nagarajan et al. [30] emphasized that Ce ion with different concentrations have ability to control the shape of CaO-ces. The Ce is proven to be a good medium due to its flexibility in localising and delocalizing electrons to widen surface area and catalytic porosity.

Referring to Fig. 3.2 (b), the structure of the Ni-Ce/CaO-ces was distributed unequally. There were fewer pores on the catalytic surface, and it was a major spherical, petal-shaped solid. The primary cause of the structural formation is likely due to the cerium oxides coverage on the nickel oxide (NiO) surface, thereby limiting the movement of the catalytic particles during thermal cracking. The oxygen vacancies are beneficial in mitigating the charge imbalance between Ni^{2+} and Ce^{3+} cations. In addition, the results from compensating for the imbalance between these rare earth metal and transition metal ions form pairs of particles made up of Ni and O_2, which can become an additional source of active sites, allowing CO_2 molecules to dissociate.

The structure of Zn-Ce/CaO-ces in Fig. 3.2(c) displayed a hollower texture and grain size of catalysts with tiny surfaces without any metal coatings. On the other hand, most of the internal particles were almost completely distributed with a cracking shape on the catalytic surface. Fe-Ce/CaO-ces (refer to Fig. 3.2(e)) and Cu-Ce/CaO-ces (refer Fig. 3.2(f)), on the other hand, were found agglomerated in various sizes. As only 1wt % metal oxide is utilised for metal-doping of Ce/CaO-ces, it is believed the cerium ion Ce^{3+}, experienced repulsion with the zinc ion, Zn^{2+}. The tendency for oxidation becomes stronger, which, in turn, results in the emission of electrons, and both elements are losing them. Therefore, the catalyst cannot maintain the mechanical strength or remain in a fixed shape; instead, the catalytic structure will end up scattered or agglomerated, which would further reduce the binding of feedstocks to the pores on the catalyst as the structure is corrupted, the pores will be completely blocked or flattened. Similarly found by J.F. Muñoz-Chilito and J.E. Rodríguez-Páez (2025) [17], the 5 wt.% loading of cerium on the zinc oxide (ZnO) catalyst will generate catalytic surface which is covered with small grains. The CO_2 molecule is believed to bind strongly to the Ce/CaO-ces, as the surfaces of zinc and oxygen vacancies can contribute to the adsorption of EFB.

The Fe-Ce/CaO-ces only displayed a few longitudinal, cylindrical morphologies, but in agglomeration (refer to Fig. 3.2(e)). Iron can beef up oxygen vacancies on the ceria surface similar to the nickel. In Table 3.1, the specific surface area and pore volume of Ni-Ce/CaO-ces are greater than those of Fe-Ce/CaO-ces. Nevertheless, metal doping with Fe surprisingly results in the formation of mesopores and macropores regardless of pore diameter [18]. Compared to nickel-based Ce/CaO-ces with a pore diameter of 23.64 nm, iron-based Ce/CaO-ces had a larger diameter of 31.29 nm. This indicates NiO compounds were coated in an unbalanced path, unexpectedly causing blockage at the centre of the pore. The Fe-Ce/CaO-ces instead, cerium mesopores and macropores found on the surface of iron oxide can facilitate the introduction of large molecules of feedstock and pyrolysis oil through pore walls with only minor undesirable byproducts are produced, for instance esters, alcohols or phenol.

The FESEM micrograph of Fe-Ce/CaO-ces and Mn-Ce/CaO-ces catalysts, as shown in Fig. 3.2(e) and 3.2(g), features an irregular, triangular shape. The particle appears to be slightly larger compared to the Ce/CaO-ces (refer to Fig. 3.2 (a)). The micropores in the catalyst are clearly visible, indicating high catalytic performance and anti-coking. The surface of the catalyst looks different from that of the CaO-ces without cerium oxide treatment. Compared to the eggshell-based catalyst with the initial dumbbell-shaped structure (refer to Fig. 2(b) in previous work), the bumpy surface of Fe-Ce/CaO-ces has a rougher

surface. Figure 3.2(e) showed that the Fe-Ce/CaO-ces possessed a higher catalytic surface area with a high possibility for reactions to take place slowly. Yusuff et. al [19] conducted a study on the influence of iron doping in mesoporous ceria for catalytic activity in styrene oxidation. They reported that the formation of Fe^{3+} ions in Ce-O-Fe solid solutions is a necessary medium to minimise crystallite size, and, in contrast, the surface area will become larger, creating more active sites. The generation of active sites can enhance lattice oxygen mobility, thereby providing additional space for oxygen storage and release, as well as enhancing the modified redox properties and the material's reducibility.

Referring to Fig. 3.2(f), the clumps of particles in an almost-cubic form, with several spaces believed to be active sites, were arranged in a line-shaped form. The formation of hydrocarbons was still lower because the EFBs were not fully adsorbed. The lead-to-process partial pyrolysis took place, with a rise in acid production. Observing surface morphology for both Co-Ce/CaO (Fig. 3.2(d)) and Cu-Ce/CaO (Fig. 3.2(f)), the structure displayed by the copper-modified CaO was comparatively smaller compared to the cobalt-modified, which could be attributed to the elemental composition of Ce_2O_3 having been reconstructed from the addition of cobalt oxide [20]. Similarly, it was reported that cobalt doping decreased the catalyst's surface area. This symbolises the successful integration of cobalt oxide as internal support for ceria. As elemental support for cerium, this also indicates the presence of cobalt in Ce/CaO-ces from surface morphology (refer Fig. 3.2(f)). From the surface morphology of all CaO-ces, it could be observed that the metal doping on catalysts by the wet impregnation approach decreases the porous density and volume of the catalytic structure. Besides, most of the structure remained intact, with less space available for the adsorption of EFB pigment onto the surface of cerium-treated CaO-ces catalyst.

3.3. Textural Properties

The Braunauer-Emmett Teller (BET) surface area, pore volume, and pore diameter for chicken eggshell-derived calcium oxide (CaO-ces) and all synthesized catalysts were tabulated in Table 3.1. The textural properties of CaO-ces were obtained from the previous work conducted by Ali et al. [7]. They reported that the surface area, pore volume, and pore diameter of CaO-ces were 8.72 m^2/g, 0.0156 cm^3/g, and 3.87 nm, respectively. As shown in Table 3.1, Ce/CaO-ces has the largest surface area, at 15.36 m^2/g. In detail, the addition of cerium as a rare earth element had significantly enhanced the surface area of CaO-ces. This may be due to the proper integration of cerium oxides with CaO-ces during calcination, which increases surface area. Similarly, Xiong et al. [21] found that adding cerium increases the support's surface area. Thus, it can be concluded that cerium is a suitable candidate to increase the support's surface area in this study.

Tevfik Aysu et al. [22] reported that adding ceria reduced the surface area and pore volume of the catalysts, while the average pore size varied little. Meanwhile, a study by Gajendiran et al. [2] on CeO_2 behaviour reported that the redox behaviour of Ce^{4+} and Ce^{3+} ions enabled them to store and release O_2 without any change in concentration under atmospheric conditions, where reduction took place.

Table 3.1
Textural properties of CaO-ces, and metal modified CaO-ces

Catalysts	**[a]S_{BET} (m^2/g)**	**[b]V_{total} (cm^3/g)**	**[c]D (nm)**
[1]CaO- ces	8.72	0.0156	3.87
Ce/CaO-ces	15.36	0.0856	22.29
Ni-Ce/CaO-ces	9.30	0.0549	23.64
Zn-Ce/CaO-ces	11.91	0.0676	22.70
Co-Ce/CaO-ces	7.04	0.0692	39.30
Fe-Ce/CaO-ces	6.63	0.0518	31.29
Cu-Ce/CaO-ces	9.09	0.0702	30.89
Mn-Ce/CaO-ces	13.83	0.0767	22.18

[1]Obtained from Ali et al. [7] with permission.

[a]S_{BET} (BET surface area) was obtained using Brunaeur-Emmett-Teller.

[b]V_{total} (total pore volume) was obtained from the adsorbed amount at $P/P_0 = 0.99$.

[c]D (pore diameter) was obtained from the adsorption branches of the isotherm by BJH method.

Unfortunately, the addition of transition metal oxides into Ce/CaO-ces had reduced the surface area. For example, the Mn-Ce/CaO-ces achieved at 13.83 m^2/g, followed by Zn-Ce/CaO-ces (11.91 m^2/g) > Ni-Ce/CaO-ces (9.30 m^2/g) > Cu-Ce/CaO-ces (9.09 m^2/g) > Co-Ce/CaO-ces (7.04 m^2/g) > Fe-Ce/CaO-ces (6.63 m^2/g). The ceria-treated chicken eggshell-based calcium oxide (Ce/CaO-ces) that was doped with Mn and Zn significantly increased the catalytic surface area, from 8.72 m^2/g (CaO-ces) to 13.83 and 11.91 m^2/g, respectively. As the electrons movement and exchange between ceria-manganese (Ce-Mn) and ceria-zinc (Ce-Zn) are expected in a controlled flow rate, a strong attraction between electrons attached to metallic particles and protons on the ceria drives the metal particles to distribute fairly throughout the surface, leaving a small portion clogged at the pore of catalyst. The metal doping with ceria successfully altered the oxygen adsorption ratio, thereby enhancing the stability of Zn-Ce/CaO-ces. As a second astonishing fact, cerium oxides present a crystal plane from 100 to 110, which contains a number of active areas that are highly exposed to collect electrons and use them for enhancing electrocatalytic activity during catalytic co-pyrolysis [23]. For BET analysis conducted on manganese-doped Ce/CaO-ces, there is a significant possibility that the area is affected due to manganese oxide (MnO) lattice expansion. This is because one of the advantages of using a manganese-based dopant is the reduction of the energy barrier. When the energy barrier turns lower, Fenton-like catalytic efficiency is enhanced [24]. To summarize, Mn-Ce/CaO-ces can lower the activation energy required for the catalytic

activities brought by Ce/CaO-ces for forming pores so that used cooking oil-treated EFB can be adsorbed and bind to the catalyst's surface to pyrolyze oil.

On the other hand, Ni-Ce/CaO-ces and Cu-Ce/CaO-ces, shared an approximately similar surface area, at 9.09 and 9.30 m^2/g, respectively. There was an exception, however, where metal doping lowered the specific surface area; for instance, the CaO catalyst modified with Co had a surface area of 7.04 m²/g, and the catalyst with Fe had an area of 6.63 m²/g. Thus, the cobalt and iron oxides did not favour the increase in the surface area of CaO-ces. This could be due to the deposition of cobalt and iron oxides on the surface of CaO-ces. In a laboratory work conducted by Li et al. [25], the addition of cobalt and iron oxides into CaO-ces causes the formation of nanocrystals. As a result, the largest macropores and mesopores disappeared, but small free volumes were then produced. Therefore, cobalt and iron oxides are believed to possess poor dopant dispersion. For another surprising fact, metal-doped catalysts had smaller pore volumes compared to the catalyst treated only with Ce. As shown in Table 3.1, it was observed that the catalyst that was metallic-doped using Ni caused a decrease in pore volume, from 0.0856 to 0.0549 cm^3/g, and a similar result from catalysts modified using Zn, Co, Fe, Cu and Mn, with the pore volume recorded at 0.0676, 0.0692, 0.0518, 0.0702 and 0.0767 cm^3/g, respectively. This might be caused by the deposition of metal oxide particles inside the porous layer. Similarly, a decrease in mesoporous volume was primarily due to the metal oxide layer covering the CaO surface, which partially blocked the catalytic channels. In conclusion, because the metal oxide particles were not evenly distributed throughout the Ce/CaO-ces, the acidic layer of metal oxides coating the Ce/CaO-ces surface occupied most active sites within the catalyst and blocked ample pore space.

For the reduction in Ni-Ce/CaO-ces pore volume as shown in Table 3.1, this result could be related to the dispersion of nickel oxide (NiO) particles or due to the blocking of NiO particles at the CaO-ces pore channels. The results obtained were completely contrary to those obtained from laboratory work conducted by Balasundram et al. [3], which stated that the treatment of Ce and addition of Ni contributed only a minor change to the CaO-ces catalytic surface area. Surprisingly, the Ni mass loading of around 4 to 5 wt.% did not result in any significant reduction in pore diameter. In this experiment, metal mass loading, which was set at 1wt %, has shown that when the ratio of Ni is lower compared to the Ce, the Ce^{3+} ions could disperse smoothly on the CaO-ces surface, resulting in the enlargement of the pore diameter. Comparing all six metallic-modified Ce/CaO-ces, the copper-modified catalyst (Cu-Ce/CaO-ces) has the lowest change in total pore volume compared to other samples, from 0.0856 cm^3/g to 0.0702 cm^3/g as indicated in Table 3.1. This is because, when carrying out pyrolysis at 500°C, the copper ions (Cu^{2+}) might enhance lattice vibration absorption and free-carrier absorption. In summary, metal doping using Cu on cerium-treated CaO-ces maintains the catalyst's textural properties and keeps the particles under stable conditions.

From Table 3.1, the pore diameter of CaO-ces was recorded at 3.87 nm. Furthermore, for an unexpected outcome, the pore diameter increased dramatically following the addition of cerium to 22.29 nm. Changes and re-modification may influence the rise in pore diameter in the presence of lattice oxygen,

metal-oxygen bonds, and the host structure of the metallic-modified catalyst. To support this, cerium oxides are a key oxide that can enhance the redox properties of CaO-ces; therefore, with the utilisation of Ce, the creation and diffusion of oxygen vacancies can occur simultaneously, allowing the lattice oxygen to become more mobile, which in turn leads to a pore diameter that enables molecules to penetrate inner pores. For the six samples of metallic CaO-ces catalysts, Co-Ce/CaO-ces possessed the highest pore diameter at 39.30 nm, followed by Fe-Ce/CaO-ces (31.29 nm) > Cu-Ce/CaO-ces (30.89 nm) > Ni-Ce/Ca-ces (23.64 nm) > Zn-Ce/CaO-ces (22.70 nm) and Mn-Ce/CaO-ces (22.18 nm). The main reason for the increase in diameter could be due to mass loading of both metal oxides at 1 wt% into Ce/CaO, which resulted in minor changes in the pore volume of CaO catalysts; hence, both pore diameters were smaller. In general, the metallic-modified Ce/CaO-ces increased both pore volume and diameter by about 7 to 10 times compared to CaO-ces and Ce/CaO-ces without any metal coating.

3.4. Pyrolysis product

In our previous work, we conducted non-catalytic co-pyrolysis of EFB and UCO at varying temperatures ranging from 400 to 700°C. We found that the hydrocarbons in pyrolysis oil increased significantly from 400°C at 4.1% to 64.9% at 650°C [10]. In this study, we developed a metal-modified calcium oxide-derived eggshell catalyst to investigate the potential for generating higher hydrocarbons at a lower temperature of 500°C compared to non-catalytic conditions at 650°C.

For pyrolysis using EFB added with UCO, but with the addition of chicken eggshell-derived calcium oxide (CaO-ces) that had been calcined at 650℃ as the catalyst. Compared to non-catalytic, pyrolysis oil percentage yield obtained from catalytic pyrolysis recorded at 48.68 wt%, 18.14 wt%, char and 33.18 wt% of non-condensable gas (refer Fig. 3.3). The chicken eggshell improved the catalytic reaction because of its moderate surface area, substantial pore volume, and a high bio-oil yield was observed. The CaO-ces is believed to intensify the cracking of the carbon chain in the EFB-UCO molecules; as a result, the thermochemical activation energy required is lowered. Metal doping using rare metal such as cerium into transition metal-modified catalysts increased the catalytic surface's basicity, and modify electrons for chemisorption of CO_2 [26]. As a result, the gas product from the thermal cracking decreased, and more pyrolysis oil was produced through the enhanced molecular cracking. Total percentage yield for oil, char and gas for different catalysts was plotted (Fig. 3.3).

There were eight catalysts utilized to compare the bio-oil produced from batch pyrolysis, which were CaO-ces, Ce/CaO-ces, Ni-Ce/CaO-ces, Zn-Ce/CaO-ces, Mn-Ce/CaO-ces, Fe-Ce/CaO-ces, Cu-Ce/CaO-ces, and Co-Ce/CaO-ces. The highest oil produced was Mn-Ce/CaO-ces, with the oil percentage yield at 73.03 wt%, followed by Cu-Ce/CaO-ces (66.05 wt%) > Co-Ce/CaO-ces (60.87 wt%) > Zn-Ce/CaO-ces (60.73 wt%) > Ni-Ce/CaO-ces (59.30 wt%) > Fe-Ce/CaO-ces (58.75 wt%) > Ce/CaO-ces (53.69 wt%) > CaO-ces (48.68 wt%). In detail, all the ceria-treated catalysts showed an increase in the production of bio-oil yield from CaO-ces at 48.68 wt%. This might be due to the ceria as a strong oxidizing agent, which lowers the secondary cracking. It is believed that cerium oxide is able to manage the donation and acceptance of electrons for oxygen circulation, which enhances oil production.

Balasundram et al. [9] demonstrated that ceria can store and release oxygen into the atmosphere within the pyrolysis tube, resulting in hydrogenation. According to Fig. 3.3, Mn-Ce/CaO-ces has achieved the highest pyrolysis oil yield of 73.03 wt% compared to other catalytic samples. This may be due to the higher surface area of Mn-Ce/CaO-ces at 13.83 m^2/g (Table 3.1), which enhances the cracking of feedstock into condensable liquid oil. Apart from that, the pore diameter of Ce/CaO-ces may not significantly be affected upon manganese-doping, which blocked the pore resulting in a decrease of pore diameter, from 22.29 to 22.18 nm (Table 3.1). A bigger pore on the catalytic surface of Mn-Ce/CaO-ces provided space for EFB covered with UCO to bind to the catalytic surface and undergo deoxygenation and carbonization for shaping of C-H bonds and promotes cracking to form liquid hydrocarbons [27]. To date, Battumur et al. [26] found that the ceria can be utilized to lower the temperature for carbon dioxide desorption peaks, for medium and strong basic sites. Nickel (Ni)-doped ceria, in which the cerium ions' oxygen vacancies are produced. Therefore, we can summarise that ample pore diameter and volume can prevent complete blockage of coke onto the catalysts and allow the deoxygenation of oil extracted from EFB to remove oxygenated components, which mainly include esters and acids.

The graph presented (refer to Fig. 3.3) further demonstrates that the catalyst has a positive impact on hydrocarbon formation. The active sites available on CaO-ces had the potential to remove water molecules from oxygenated compounds through various processes, including dehydration and hydrolysis, as reported by Hakim et al. [28]. The presence of basic active sites also represents a high surface contact frequency between CaO-ces and feedstocks (EFB and UCO), resulting in a moderately high composition of hydrocarbons (mostly alkanes and alkenes, ranging between 13.18 and 39.43 wt%). For biochar production from catalytic co-pyrolysis, biochar resulted from the pyrolysis with ordinary CaO-ces at 18.14wt %. For a more astonishing fact, catalytic enhancement by transition metals improves the reaction by lowering the mass percentage yield of black solidified chars to below that CaO-ces, from the highest to the lowest for pyrolysis of feedstocks using Zn-Ce/CaO-ces (18.06wt%) > Fe-Ce/CaO-ces (17.92wt %) > Ce/CaO-ces (17.70wt %), Co-Ce/CaO-ces (17.03wt %), Cu-Ce/CaO-ces (16.32wt %), Ni-Ce/CaO-ces (15.60wt %), and Mn-Ce/CaO-ces (9.83wt %). Based on the percentage yield described above, the addition of Mn enhances the gasification and pyrolysis process, breaking down most of the solid feedstocks into gaseous byproducts and liquid hydrocarbon oils. Similar to the gas release, the addition of transition metals enables the accumulation of hydrocarbons into a final liquid form, rather than being released into the atmosphere as non-condensable gases. From the catalytic co-pyrolysis of feedstocks, the gaseous products obviously decrease from reaction using CaO-ces (33.18wt %), to 28.61wt % by cerium-added CaO-ces. Metal-doping made into the Ce/CaO-ces has been indirectly influencing the number of electrons presented, benefiting the pyrolysis by reduction in the gas product's yield, with the gas formed reduced respectively to 25.11wt % (Ni-Ce/CaO-ces), 23.33wt % (Fe-Ce/CaO-ces), 22.09wt % (Co-Ce/CaO-ces), 21.21wt % (Zn-Ce/CaO-ces), 17.62wt % (Cu-Ce/CaO-ces), and 17.14wt % (Mn-Ce/CaO-ces). The illustrated graph in Fig. 3.3 clearly shows that manganese exhibits good properties as an electron regulator, indicating a suitable medium for carrying out and modifying oxidation and reduction reactions.

3.4.1. Organic compositions in pyrolysis oil

For the organic compounds presented using different catalysts for conducting pyrolysis, the percentage yield for different compounds was tabulated in Table 3.2 and further illustrated in a graph in Fig. 3.4. In our previous work [10], we observed the gradual increase in hydrocarbons yield in pyrolysis oil at a temperature 500°C without a catalyst, recorded at 3.1 wt.%. Interestingly, in our previous results at 500°C, the hydrocarbons yield was recorded at 3.1 wt% from the non-catalytic co-pyrolysis of EFB and UCO. But with the addition of CaO-ces in this experiment, it significantly maximizes the total yield of hydrocarbons, at 13.18wt % at the same temperature.

Table 3.2
Organic compounds composition in pyrolysis oil.

Catalysts Type	CaO-ces	Ce/CaO-ces	Ni-Ce/CaO-ces	Zn-Ce/CaO-ces	Mn-Ce/CaO-ces	Fe-Ce/CaO-ces	Cu-Ce/CaO-ces	Co-Ce/CaO-ces
Hydrocarbons	13.18	25.63	20.64	39.43	38.24	34.05	22.10	35.04
Acids	61.38	34.24	40.22	21.68	37.58	33.05	44.02	31.36
Esters	14.76	13.13	18.90	21.60	12.31	15.16	19.10	13.10
Phenols	2.44	12.58	4.55	3.88	2.65	8.01	5.48	3.74
Ketones	3.86	6.25	6.24	5.39	2.61	5.97	6.31	8.24
Alcohols	1.79	5.67	3.80	3.97	0.69	4.13	3.34	3.54
Aldehydes	2.64	3.21	2.09	2.76	0.68	1.67	2.67	3.80

From Table 3.2, it was observed that the hydrocarbon percentage yield in pyrolysis oil using EFB and UCO with CaO-ces achieved the lowest value, at 13.18 wt%. Different from the CaO-ces, catalysts that were treated with ceria displayed a higher yield of hydrocarbons. A study by Nagarajan et al. [30] stated that the presence of multiple oxidation states, facile electron transfer, and mild acid-based nature in redox metal oxides results in the production of several active catalytic surfaces, which can boost liquid bio-oil production [28]. For the oil produced by applying metal-doped catalysts, the highest hydrocarbon coverage was recorded by Zn-Ce/CaO-ces with a percentage yield at 39.43 wt%, followed by Mn-Ce/CaO-ces (38.24 wt%) > Co-Ce/CaO-ces (35.04 wt%) > Fe-Ce/CaO-ces (34.05 wt%) > Ce/CaO-ces (25.63 wt%) > Cu-Ce/CaO-ces (22.10 wt%) > Ni-Ce/CaO-ces (20.64 wt%). Ce/CaO-ces doped with Zn is believed to be driven by filling of zinc d-orbitals with electrons, which is helpful in adsorption and hydrogen activation [29]. To further elaborate on the reason for better conversion from EFB and UCO into hydrocarbons, its porous surface and higher surface area per volume ratio contribute significantly, as judged from the surface morphology (refer to Fig. 3.2 (c)) conducted through FESEM. In contrast, the Ni-Ce/CaO-ces did

not possess many pores and sites for feedstock adsorption, hence less hydrocarbons (20.64 wt% %) were produced from co-pyrolysis.

From the textural properties study conducted using BET, the surface area and volume of porous sites on Zn-Ce/CaO-ces (11.91m^2/g and 0.0676 cm^3/g) outweighed Ni-Ce/CaO-ces (9.30 m^2/g and 0.0549 cm^3/g), which supports thermal conduction into the core of feedstock and catalytic particles to move vigorously and increase in kinetic motion. Therefore, more oil was pyrolyzed (60.73wt % oil yield from pyrolysis of feedstock using Zn-Ce/CaO-ces) via a catalyst-supported heat treatment process. The next concentrating point will be the highest oil conversion through the addition of Mn-Ce/CaO-ces, which was recorded at 73.03 wt% based on Fig. 3.3. Mn metal is favourable for cerium equivalent dispersion across the whole surface of Ce/CaO-ces. To prevent the breakdown of the surface of the catalyst due to an intermediate switch in pH. Apart from that, despite a less active surface at XRD peaks compared to Fe-Ce/CaO-ces, Mn-Ce/CaO-ces has comparatively higher textural properties. Third point, before the addition of cerium into CaO-ces, the pyrolysis oil was recorded at 48.68 wt.% (Fig. 3.3). However, the rise in oil yield (53.60 wt.%) was one of the contributions cerium had made, which protects the surface layer of basic nature of CaO-ces from neutralized when in contact with acidic nature of transition metals, and besides allows metals to converge and construct hard, stable CaO-based structure. With the catalysis pre-treatment using cerium oxide (CeO_2), cerium's catalytic surface became more stable and resistant to high temperatures, preventing the accumulation of powder particles into clumps. The component that is responsible for the redox reaction by Ce is oxygen vacancies inside CeO_2. It is coupled with polarons, assisting the storage and release of O_2 easily by localization and delocalization of electrons on cerium ions to form Ce^{3+} sites. Therefore, ceria could convert the oxygen-rich components into ketonic-rich mono-functional molecules, for production of more hydrocarbons within bio-fuel. Higher surface concentration of Ce^{3+} in CeO_2 indicates that more surface-active sites are produced; therefore, catalytic activity for pyrolysis between EFB and UCO will become faster and active.

Based on Table 3.2, the CaO-ces catalysts modified with Zn and Mn achieved the highest yield of hydrocarbons. One reason is the higher surface area, at 11.91 and 13.83 m²/g, respectively. We can assume that a surface area between 11 and 14 m²/g is the ideal surface area for thermal cracking at the maximum rate, allowing more hydrocarbons to be pyrolysed from EFB mixed with UCO. The two transition metals mentioned are all categorized as reducing agents. The use of a reducing agent can increase the oxidation state of the catalyst, as Ce/CaO-ces donates electrons, while oxygen is emitted into the surroundings. As a result, the oil formed mainly contains carbon and hydrogen, and the oxygen is mixed with a small portion of EFB to form oxygenates such as phenols, esters, ketones, and other minor side components. Besides hydrocarbons, the presence of oxygenated compounds, such as alcohols, esters, aldehydes, ketones, acids, and phenols, as side products indicates that O_2 atoms can still be found in oil in lower yields. This demonstrates that CaO-ces can undergo cycles of decarbonylation, decarboxylation, and dehydration simultaneously.

For phenols percentage in pyrolysis oil, referring to Table 3.2, pyrolysis oil using eggshell (CaO-ces) without ceria had a percentage yield recorded at 2.44 wt.%. The results revealed that the production of phenols from the co-pyrolysis of EFB and UCO, using CaO-ces treated with ceria, increased to 12.58 wt%. This proved that the addition of ceria could boost the production of phenol, as most oxygen is absorbed and stored inside the CE, while the remaining oxygen is used in the pyrolysis process. From a previous study on selective production of monomeric alkyl phenols from Kraft lignin's hydrogenolysis conducted by Chen et al. [29], the oxygen atoms adsorbed on the catalyst's voids modified using metal oxides, enchanting the C-O bond, promoting more production of phenols inside bio-oil pyrolyzed. Comparing the phenol yield within the catalysts with different transition metals, the Fe-Ce/CaO-ces recorded the highest yield (8.01wt %), followed by Cu-Ce/CaO-ces (5.48wt %) > Ni-Ce/CaO-ces (4.55wt %) > Zn-Ce/CaO-ces (3.88wt %) > Co-Ce/CaO-ces (3.74wt %) > Mn-Ce/CaO-ces (2.65wt %). This may be affected by phenol degradation during the thermal cracking process. Zheng et al. [31] found that the differences in the ratio in which cerium is lower than Mn at 2:8wt% % would cause the formation of Ce/Mn solid solution. As the cerium ions enter the cerium oxide (CeO_2) crystal lattice, Mn redox properties will be reduced slowly, and the catalytic behaviour of Mn will be slowed down. Therefore, in Table 3.1 for the BET analysis, we can observe that the catalytic surface area decreases slightly from 15.36 m^2/g to 13.83 m^2/g after modification with Mn. The total hydrocarbons and oxygenated compounds in pyrolysis oil from all catalytic samples were summarized in Fig. 3.4.

From our previous work there was no liquid hydrocarbons contained in the oil pyrolyzed by utilizing only EFB at 500°C, in contrast concentrated hydrocarbons were recorded from the sample pyrolyzed from UCO, at 82.2wt %. Co-pyrolysis conducted on both EFB and UCO at 500°C computed a lower yield of hydrocarbons at 3.1wt.% which was comparatively lower than pyrolysis oil from catalytic co-pyrolysis using CaO-ces at 13.18 wt.% where 4.3 times more hydrocarbons were formed. Acidic-based oil in EFB, since bunches of hydrogen bonds firmly bind it, the hydrocarbons were not completely removed. Still, instead some unseparated carbon and hydrogen remained clumped to react with oxygen to form oxygenated compounds as listed in Table 3.2. The formation of acid is the highest compared to hydrocarbons and other oxygenates. The acid in pyrolysis oil produced using chicken eggshell-derived calcium oxide (CaO-ces) contained up to 61.38wt %. The percentage of acid in pyrolysis oil dropped to 34.24 wt.% after the CaO-ces modified with cerium. Similar reduction in the range of 21.68 to 44.02 wt.% can be observed for bimetallic modified CaO-ces as shown in Table 3.2. We observed that Cu-Ce/CaO-ces had the highest acid yield recorded at 44.02 wt.%, followed by Ni-Ce/CaO-ces (40.22 wt.%), Mn-Ce/CaO-ces (37.58 wt.%), Fe-Ce/CaO-ces (33.05 wt.%), Co-Ce/CaO-ces (31.36 wt.%) and Zn-Ce/CaO-ces (21.68 wt.%). By mixing acid from metal oxide into the Ce/CaO-ces, acidity in metal oxide compounds will react vigorously with calcium oxide which possesses basic nature to break down the acids into hydrocarbons more effectively and faster. The CaO-ces catalyst also accelerates the deoxygenation of triglycerides, promoting decarboxylation and deoxygenation process [19]. When referring to the surface morphology of Cu/Ce-CaO-ces, Ni/Ce-CaO-ces, and Mn/Ce-CaO-ces (refer to Fig. 3.2d, 3.2h, and 3.2i), we can observe that the pores formed on the catalysts are fewer and smaller. They did not possess a regular, fixed shape, with smaller pore volumes of 0.0702, 0.0549, and 0.0767 cm^3/g, respectively. It not

only reduces the sites for tolerating acid and dissociates them into hydrocarbons, but at the same time increases the acidity properties. Hence, it makes sense if the mass of the manganese oxide, nickel oxide, and copper oxide used in metal-doping during catalyst making is more than the respective mass of cerium oxides, leading to the generation of more Lewis-acid strength. The percentage of esters found in different pyrolysis oils is almost the same. According to Table 3.2, the initial yield of esters in CaO-ces without any Ce_2O_3 treatment was up to 14.76 wt.%. However, a fluctuation in the lignocellulosic components in EFB occurred when ceria was introduced into the feedstock. In return, a slight decrease in ester yield to approximately 13.13 wt.%. The interesting part is that most metal oxides favour and encourage the esterification process. Referring to Table 3.2, Zn-Ce/CaO-ces produced esters at 21.60 wt.%, followed by Cu-Ce/CaO-ces (19.10 wt.%), Ni-Ce/CaO-ces (18.90 wt.%), Fe-Ce/CaO-ces (15.16 wt.%), Co-Ce/CaO-ces (13.10 wt.%), and Mn-Ce/CaO-ces (12.31 wt.%). A metal support catalyst is an appropriate medium for modification, as it exhibits unique properties in wet impregnation, which can provide and promote a strong metal-support interaction. Referring to the statement taken from an article regarding a study on the addition of cerium to nickel [30], the cerium ions presented in cerium oxides can regulate interfaces between the metal and its support, distributing metallic components throughout the CaO-CeO2 surface. This leads to a more effective facile switching between Ce^{3+} and Ce^{4+} ions for transferring electron charge to the deposited metal species. And from there, carbohydrates, furans, and lignin can undergo hydrolysis. From Table 3.2, it is found that Ce/CaO-ces modified using zinc, copper, nickel, and iron favour the esterification process. The addition of cobalt into the catalyst did not create either a dramatic increase or a decrease in the ester's formation, and the manganese-doped catalyst reduced the ester compounds in the pyrolysis oil.

In Table 3.2, an increment from 3.86 to 6.25 wt.% of ketones with the CaO-ces was treated with ceria. After that, we could deduce that the redox properties of cobalt were stronger, resulting in the formation of more ketones. It can be described that the cobalt creates a path for hydrogen atoms to be adsorbed at the surface of CaO-ces, allowing for the conversion of alcohols into ketones. On the other hand, Ni and Cu are neutralizing as they did not bring too many changes in the ketones production. In the decreasing order, the highest production of ketones were at Co-Ce/CaO-ces (8.24 wt.%), and accompanied by Cu-Ce/CaO-ces (6.31 wt.%) > Ce/CaO-ces (6.25 wt.%) > Ni-Ce/CaO-ces (6.24 wt.%) > Fe-Ce/CaO-ces (5.97 wt.%) > Zn-Ce/CaO-ces (5.39 wt.%) > CaO-ces (3.86 wt.%) > Mn-Ce/CaO-ces (2.61 wt.%). The CaO-ces catalyst accelerates the deoxygenation of triglycerides, converting oxygen for ketones production [10]. At the surface area of cerium oxide (Ce_2O_3), it is used for catalytic centres to stabilize carboxylates. Similarly, the strength shown by the hydrogen atom (H) and Ce/CaO-ces will crucially affect the production of alcohol, which then undergoes dehydration or hydrogenation to form ketones as more basic sites continue to be created [31]. A catalytic collision between CaO-ces and $_{H2}$ atoms accumulated in pyrolysis oil will actively enhance the feedstock pyrolysis process, resulting in the formation of more ketones. Although operating in an environment with high acidity, the CaO-ces advantage in the release and absorption of electrons makes the catalyst less prone to deactivation. In conclusion, compared to noble metals, the metal oxides possess high anti-deactivation properties [32].

Besides ketones, other oxygenates present in pyrolysis oil are aldehydes as feedstocks, EFB, and UCO have carbonyl functional groups. A similar observation was found, where the thermal degradation of hemicellulose on the cellulose surface of biomass may be the cause of the increased generation of hemicellulose-derived products, such as aldehydes. Referring to Table 3.2, in the absence of ceria, the aldehydes in the pyrolysis oil sample using pure CaO-ces were 2.64 wt.%. Following the addition of ceria, there was a slight increase in the oxidation decarboxylation rate, which resulted in the aldehyde yield rising from 2.64 to 3.21 wt.% due to the improvement in oxygen vacancies at the catalytic surface of Ce/CaO-ces. Except for the Co-Ce/CaO-ces catalyst, which is more biased towards aldehydes production, the percentage yield in other catalysts engineered with transition metals marked a moderate drop in aldehydes production. Referring to Table 3.2, the pyrolysis oil using Zn-Ce/CaO-ces had the highest yield of 3.80wt %, accompanied by Ce/CaO-ces (3.21 wt.%) > Zn-Ce/CaO-ces (2.76 wt.%) > Cu-Ce/CaO-ces (2.67 wt.%) > CaO-ces (2.64 wt.%) > Ni-Ce/CaO-ces (2.09 wt.%) > Fe-Ce/CaO-ces (1.67 wt.%) > Mn-Ce/CaO-ces (0.68 wt.%). This may be due to the partial oxidation experienced by organic molecules, which results in the formation of aldehydes. As UCO contains fatty acids, at a pyrolysis temperature of 500°C, the hydrogen bond (H-H) is degraded thermally. Comparable research by Shah et al. [14] found that aldehydes are formed when fatty acids in UCO break down. The breaking of ester bonds in an environment with high temperature, without any oxygen present, degrades the compounds into smaller molecules. Aldehydes can be produced by subsequent heat degradation of these molecules. Aldehyde formation at 500°C was the highest within the sample reacted with Ce/CaO-ces modified using Zn. From Fig. 3.1, referring to the XRD graph of CaO-ces pattern and metal-doped CaO-ces, peaks for Zn-Ce/CaO-ces at 2θ = 78.34° and 80.65°. Shaping of mesoporous region at the surface of Ce/CaO-ces (refer Fig. 3.1) that are modified using Zn shows that new points on CaO-ces built up with crystalline along with new spots filled with pores for blended EFB binding at the active site, beside more active area can be openly exposed to the heat sources inside FBR for slow heating, gradually rising in temperature until reaches 500°C [33]. To summarize the performance of catalyst on pyrolysis oil production, the work carried out indicates that ceria-layered CaO-ces could protect the surface layer of the basic catalyst by preventing its surface from dissemble due to neutralization upon addition of transition metal oxide layer (refer Fig. 3.2 (c)).

3.4.2. Hydrocarbons range in pyrolysis oil

The hydrocarbons in pyrolysis oil can be categorized into three groups based on their ranges. For example, light hydrocarbons, also known as light naphtha, are hydrocarbons (C5 to C9), mid hydrocarbons (C10-C16), and heavy hydrocarbons, also known as reduced crude, which range from C17 and above, as shown in Table 3.3. From previous work [10], C_7 (1.0 wt.%) was the only light hydrocarbon recorded at a temperature of 500°C for co-pyrolysis. And out of expectations, the pyrolysis oil sample generated using CaO-ces and cerium-treated CaO-ces did not produce any light hydrocarbons. In contrast, light hydrocarbons were only discovered in samples using cerium-treated CaO-ces and further metal-doped with transition metals. However, compared to the non-catalytic sample (1.0 wt.%), light hydrocarbons from oil collected using catalytic samples that involved nickel, zinc, cobalt, iron, and copper-doped catalysts did not support mass production of light hydrocarbons, with a yield of less than

1.0 wt.% light hydrocarbons. Surprisingly, manganese (Mn)-doped Ce/CaO-ces beefed the production of more than 3.32 wt.% (refer to Table 3.3). Ahmad et. al [34] emphasized that heterogenized manganese-based catalyst possessed the capability to dehydrogenate alcohols to the corresponding carbonyl compounds, and simultaneously performed condensation with carbonyl followed by hydrogenation reaction to produce liquid hydrocarbons.

Table 3.3
Percentage yield of total hydrocarbons in pyrolysis

Catalytic Samples	**Total Hydrocarbons (%)**	**Light Hydrocarbons (C_5 to C_9)**	**Mid Hydrocarbons (C_{10} to C_{16})**	**Heavy Hydrocarbons (C_{17} and above)**
CaO-ces	13.18	-	7.18	6.00
Ce/CaO-ces	25.63	-	18.61	7.02
Ni-Ce/CaO-ces	20.64	0.23	13.37	7.04
Zn-Ce/CaO-ces	39.43	0.59	27.68	11.16
Co-Ce/CaO-ces	35.04	0.88	26.53	7.63
Fe-Ce/CaO-ces	34.05	0.61	24.82	8.62
Cu-Ce/CaO-ces	22.10	0.38	15.64	6.08
Mn-Ce/CaO-ces	38.24	3.32	23.83	11.09

From Table 3.3, a surprising fact can be observed: pure CaO-ces and CaO-ces after being treated with ceria did not contain any light hydrocarbons. For the catalysts doped with transition metal oxides, light hydrocarbons were present in the pyrolysis oil. Mn-Ce/CaO-ces recorded the highest yield of light hydrocarbons at 3.32 wt.%, followed by Co-Ce/CaO-ces (0.88 wt.%) > Fe-Ce/CaO-ces (0.61 wt.%) > Zn-Ce/CaO-ces (0.59 wt.%) > Cu-Ce/CaO-ces (0.38 wt.%) > Ni-Ce/CaO-ces (0.23 wt.%). It can be influenced by amorphous active sites, to which EFB can attach to the pores of the catalyst to form light hydrocarbons. In Fig. 3.1, the Mn-Ce/CaO-ces experienced a higher peak at degrees 2θ of 19.07°, 27.67°, 34.02°, 48.21°, 51.08°. It was discovered that minimum metal oxide loading up to 1 wt.% potentially contributed to maximize metal oxide nanoparticles distribution and stabilization. The mesoporous cobalt oxide (CoO) with respective oxygen vacant sites because of suppressed activity for water gas shift reaction [18]. Besides, from Table 3.3, we can also read that there is an increase in the production yield of kerosene in CaO-ces treated using ceria and metallic-modified. The introduction of acids onto minor acid sites of Ce_2O_3 promotes thermal degradation, inducing an increase in the heat produced [24].

Additional heat supplied to the catalyst excites the electrons and atoms to move vigorously and expands the internal space of CaO-ces, therefore, hydrocarbons with carbon atoms between 10 and 16 were in large quantities.

Besides, for the acid concentration in pyrolysis oil (refer to Table 3.2), pyrolysis runs using pure CaO-ces without any ceria treatment and metal-doping possessed more than 50 wt.% of acids. This can be due to the small changes in the acid concentration gradient. As the calcium eggshell is basic in nature, it is considered not more substantial to trigger a sequence of events which can boost up the aromatic compounds production for instance cyclization, isomerization, and Diels-Alder reactions. Cyclization took place within ring-structured compounds, for isomerization which refers to the conversion of an isomer into a new form. For the Diels-Alder reaction, this is a cycloaddition reaction responsible to produce cyclic compounds. Three reactions mentioned can indirectly reduce the production of straight-chain hydrocarbons [35]. Therefore, as shown in Table 3.2, the addition of a basic ceria-based layer onto the CaO-ces surface can increase the catalyst's resistance to deactivation due to coking, while also allowing oxidation and reduction processes to be repeated simultaneously, thereby boosting hydrocarbon production by up to 25.63 wt.%. However, the addition of transition metals will be another consideration, as some metals, such as Cu (20.64 wt.%) and Ni (22.10 wt.%), unexpectedly lead to agglomeration due to their relatively low concentrations. Based on their surface morphology (refer to Fig. 3.2 d and h), pores and spaces between the cracks are not abundant, which reduces the probability for pyrolysis to occur. Mn is the element located in group 7 in the first row of the transition metals category in the periodic table, hence it tends to lose one electron to achieve a stable chemical structure. To further support the statement, Chang 2014) [36] said as an active metal, Mn often exhibits complex behaviours and synergistic catalytic properties, following the activities from the contact of Mn with Ce which can maintain both Mn and Ce particles in a fixed arrangement without any changes in position. Donating an electron leads to a greater deoxygenation process, stabilizing the polymerization of aromatic rings for liquid hydrocarbons production.

Conclusion and Perspectives

This study evaluated chicken eggshells-based calcium oxide (CaO-ces) for the catalytic pyrolysis of oil palm-based biomass, specifically empty fruit bunch (EFB), mixed with used cooking oil (UCO), to assess the liquid hydrocarbons produced. The textural properties of CaO-ces were studied through XRD for amorphous structure and degree of crystallization, FESEM for surface morphology, and the BET method for computing surface area, pore volume and pore diameter of the catalysts. The study also emphasizes relevance of calcium oxide in the eggshell, which serves as a base catalyst, accelerating the pyrolysis reaction and raising rate of synthesis of aliphatic hydrocarbons, the primary products of pyrolysis oil. From the overall laboratory work, it can be summarized that the introduction of cerium oxide (Ce_2O_3), improves and favours the liquid hydrocarbons production more than non-condensable gas. Metal-doping on CaO-ces catalyst is proven able to increase the percentage yield, with the pyrolysis oil using Mn-Ce/CaO-ces has the greatest yield, marked at 73.03 wt.%, with less gas emitted, recorded at 17.14 wt.%.

Based on the comparison of hydrocarbon concentration, Zn-Ce/CaO-ces recorded as oil, with the highest percentage of liquid hydrocarbons at 39.43 wt.%.

To summarize the research, which concentrates on the production of biofuel using a mixture of EFB and UCO in a ratio of 1:1 and studies the influence given through the addition of bimetallic modified CaO-ces catalysts for condensation of the liquid hydrocarbon inside at the same temperature (500°C). It contributes significantly to the advancement of catalyst technology and introduces a new step in biomass conversion. These discoveries mark the transition towards bio-catalyst development from biomass, to invent environmentally friendly, sustainable, affordable, and feasible CaO-ces. On the other hand, the co-pyrolysis of EFB marks another milestone, proving that agricultural biomass feedstock can be utilised as a source of biofuel.

The research initially concentrated on evaluating the physicochemical properties of CaO-ces catalyst based on amorphous structure, specific surface area, pore volume, pore density, pyrolysis oil percentage yield and hydrocarbons content in a pyrolysis oil sample from co-pyrolysis of EFB and UCO over ceria-treated, metallic-modified CaO-ces catalyst using nickel, zinc, iron, manganese, copper and cobalt. The studies demonstrated that the addition of the metal-modified Ce/CaO-ces enhanced the production of liquid hydrocarbons in the pyrolysis oil. Besides, it had been proven that the addition of metal into Ce/CaO-ces could reduce the non-condensable gas formed from the pyrolysis, and more gases were converted into liquid hydrocarbons. However, the production yield showed higher acid content than the liquid hydrocarbons. For future research, improvements in pyrolysis temperature beyond the current 500°C can be explored, as this laboratory work treated the temperature as a constant. As a result, the insufficiency in heating did not allow for thermal cracking, which could convert the acids into hydrocarbons and other aromatic compounds.

Abbreviations

Abbreviations	Full Form
BET	Braunauer Emmett Teller
CaO	Calcium Oxide
CaO-ces	Chicken Eggshell-derived Calcium Oxide
CE	Chicken Eggshell
Ce $(NO_3)_3.6H_2O$	Cerium (III) Nitrate Hexahydrate
CeO_2	Cerium Oxide
Co $(NO_3)_2.6H_2O$	Cobalt (II) Nitrate Hexahydrate
Cu	Copper
Cu $(NO_3)2.3H_2O$	Copper (II) Nitrate Trihydrate
EFB	Empty Fruit Bunch
Fe	Iron
Fe $(NO_3)_3.9H_2O$	Iron (III) Nitrate Nonahydrate
FESEM	Field Emission Scanning Electrons Microscopy
GC/MS	Gas Chromatography/Mass Spectrometry
GHG	Greenhouse Gas Emission
HZSM-5	Hydrogen-based Zeolite Socony Mobil-5 (HZSM-5)
IWI	Incipient Wetness Impregnation
Mn	Manganese
Mn $(NO_3)_2.4H_2O$	Manganese (II) Nitrate Tetrahydrate
Mo	Molybdenum
Ni	Nickel
Ni $(NO_3)_2.6H_2O$	Nickel (II) Nitrate Hexahydrate
NiO	Nickel Oxide
UCO	Used Cooking Oil
XRD	X-Ray Diffraction
Zn	Zinc
Zn $(NO_3)_2.6H_2O$	Zinc Nitrate Hexahydrate

Declarations

Declaration of competing interest

The authors declare that they have no known competing financial interests or personal relationships that could have appeared to influence the work reported in this paper.

Funding

Declaration

This research was funded by Universiti Teknologi Malaysia (UTM) under the Potential Academic Staff (PAS) scheme (Cost Center No.: Q.K130000.2743.03K72). The funder had no role in study design, data collection and analysis, decision to publish, or preparation of the manuscript.

Author Contribution

Yaw Huei Yat: Writing - original draft, Writing - review & editing, Visualization. Vekes Balasundram: Supervision, Conceptualization, Methodology, Funding acquisition. Norazana Ibrahim: Project administration, Supervision. Ruzinah Isha: Software, Conceptualization. Le Kim Hoang Pham: Writing – review & editing. Suan Shi: Writing – review & editing.

Acknowledgement

A special thanks to Malaysia-Japan International Institute of Technology (MJIIT), Universiti Teknologi Malaysia (UTM), for the financial support and opportunity to carry out this research project under the Final Year Project scheme.

Data Availability

The data will be made available on reasonable requests by corresponding author.

References

1. Rashidi, N. A., Chai, Y. H. & Yusup, S. Biomass Energy in Malaysia: Current Scenario, Policies, and Implementation Challenges. *Bioenergy Res.* 15. https://doi.org/10.1007/s12155-022-10392-7 (2022).
2. Gajendiran, M. et al. Surface oxygen vacancy vs oxygen storage capacity in cubic ceria based nanocatalysts for low temperature catalytic combustion of fuels. *J. Ind. Eng. Chem.* **139**, 434–443.

https://doi.org/10.1016/j.jiec.2024.05.018 (2024).

3. Vekes Balasundram, Ibrahim, N., Md, R., Kasmani, R., Isha, M. & Hasrinah Hasbullah. Catalytic pyrolysis of sugarcane bagasse using molybdenum modified HZSM-5 zeolite. *Energy Procedia*. **142**, 793–800. https://doi.org/10.1016/j.egypro.2017.12.128 (2017).
4. Queiroz, T. & Nilson, J. Evaluation of the potential use of chicken eggshell waste to manufacture dense/porous bi-layered red floor tiles. *Constr. Build. Mater.* **447**, 138117–138117. https://doi.org/10.1016/j.conbuildmat.2024.138117 (2024).
5. Ashine, F. et al. Biodiesel production from Argemone mexicana oil using chicken eggshell derived CaO catalyst. *Fuel* **332**, 126166. https://doi.org/10.1016/j.fuel.2022.126166 (2023).
6. Ali, V., Balasundram, K., Shameli, Ibrahim, N., Isha, R. & Manan, Z. A. The Effect of Calcium Oxide from Waste Chicken Eggshell on HZSM-5. DOAJ (DOAJ: Directory of Open Access Journals). (2021). https://doi.org/10.3303/cet2189031
7. Atif, M. et al. Manganese-doped cerium oxide nanocomposite as a therapeutic agent for MCF-7 adenocarcinoma cell line. *Saudi J. Biol. Sci.* **28** (2), 1233–1238. https://doi.org/10.1016/j.sjbs.2020.12.006 (2021).
8. Vekes Balasundram, K. K. et al. Catalytic upgrading of pyrolysis vapours over metal modified HZSM-5 via in-situ pyrolysis of sugarcane bagasse: Effect of nickel to cerium ratio on HZSM-5. *J. Anal. Appl. Pyrol.* **134**, 309–325. https://doi.org/10.1016/j.jaap.2018.06.021 (2018).
9. Balasundram, V. et al. A., Thermogravimetric catalytic pyrolysis of high-density polyethylene over iron modified chicken eggshell wastes. Materials Today: Proceedings, 110, 15–19. (2024). https://doi.org/10.1016/j.matpr.2023.08.041
10. Vekes Balasundram, N. A. et al. THE EFFECT OF *Jurnal Teknologi*, **87**(4). https://doi.org/10.11113/jurnalteknologi.v87.23147 (2025).
11. Ha, H. A., Al-Ansari, M. M., Al-Dahmash, N. D., Krishnan, R. & Shanmuganathan, R. In vitro analyses of cerium oxide nanoparticles in degrading anthracene/fluorene and revealing the antibiofilm activity against bacteria and fungi. *Chemosphere* **345**, 140487. https://doi.org/10.1016/j.chemosphere.2023.140487 (2023).
12. Lupa, J. et al. Ethanol steam reforming for hydrogen production over cobalt catalyst supported on the cerium oxide prepared via the one-step hard template method. *Chem. Eng. J.* 156101–156101. https://doi.org/10.1016/j.cej.2024.156101 (2024).
13. Han, Z. K., Liu, W. & Gao, Y. Advancing the Understanding of Oxygen Vacancies in Ceria: Insights into Their Formation, Behavior, and Catalytic Roles. JACS Au, 5(4), 1549–1569. (2025). https://doi.org/10.1021/jacsau.5c00095 (13).
14. Shah, P. M., Bailey, L. A., Jiang, Z., Morgan, D. J. & Taylor, S. H. The effect of washing on improving activity of co-precipitated ceria manganese oxide catalysts for volatile organic compound total oxidation. *Mol. Catal.* **573**, 114796. https://doi.org/10.1016/j.mcat.2024.114796 (2025).
15. None Supriyanto, Päivi, Y. & Richards, T. Gaseous products from primary reactions of fast co-pyrolysis of wood and plastic: the effect of CaCO3. *J. Anal. Appl. Pyrol.* **191**, 107182–107182.

https://doi.org/10.1016/j.jaap.2025.107182 (2025).

16. Windarti, T. et al. Development of calcium phosphate cement composed of silica-modified hydroxyapatite, cerium oxide, and silica as an osteoporotic bone filler. *Ceram. Int.* **50** (22), 45957–45968. https://doi.org/10.1016/j.ceramint.2024.08.437 (2024).
17. Muñoz-Chilito, J. F. & Rodríguez-Páez, J. E. Potential use of zinc oxide (ZnO) ceramic pieces doped with ceria (CeO2) or magnesia (MgO) in the reduction of polluting gases emitted by motorcycles. *Ceram. Int.* https://doi.org/10.1016/j.ceramint.2025.01.470 (2025).
18. Ensie, B. & Morteza Esfandyari. Biodiesel Production by Iron Oxide Supported on Light Weight Expanded Clay Aggregate (Fe2O3-f-LECA) Catalyst: Box-Behnken Design-Based Optimization and ANFIS Modelling with GA and PSO. *Renew. Energy*. 123466–123466. https://doi.org/10.1016/j.renene.2025.123466 (2025).
19. Yusuff, A. S., Gbadamosi, A. O. & Atray, N. Development of a zeolite supported CaO derived from chicken eggshell as active base catalyst for used cooking oil biodiesel production. *Renew. Energy*. **197**, 1151–1162. https://doi.org/10.1016/j.renene.2022.08.032 (2022).
20. Nisar, J. et al. Thermo-catalytic decomposition of walnut shells waste over cobalt doped cerium oxide: Impact of catalyst on kinetic parameters and composition of bio-oil. *Chem. Eng. Sci.* **282**, 119355–119355. https://doi.org/10.1016/j.ces.2023.119355 (2023).
21. Xiong, J. et al. Production of bio-oil from waste cooking oil via microwave-assisted pyrolysis in the presence of waste eggshell CaO and HZSM-5: Process optimization and catalyst lifetime exploration. *Energy* **283**, 128416. https://doi.org/10.1016/j.energy.2023.128416 (2023).
22. Tevfik Aysu, Fermoso, J. & Sanna, A. Ceria on alumina support for catalytic pyrolysis of Pavlova sp. microalgae to high-quality bio-oils. *J. Energy Chem.* **27** (3), 874–882. https://doi.org/10.1016/j.jechem.2017.06.014 (2018).
23. Fronzi, M., Soon, A., Delley, B., Traversa, E. & Stampfl, C. Stability and morphology of cerium oxide surfaces in an oxidizing environment: A first-principles investigation. *J. Chem. Phys.* **131** (10). https://doi.org/10.1063/1.3191784 (2009).
24. Li, H. et al. Unique electron reservoir properties of manganese in Mn (II)-doped CeO2 for reversible electron transfer and enhanced Fenton-like catalytic performance. *Appl. Surf. Sci.* **502**, 144295–144295. https://doi.org/10.1016/j.apsusc.2019.144295 (2019).
25. Li, K. et al. Tandem pyrolysis-catalytic upgrading of plastic waste towards kerosene-range products using Si-pillared vermiculite with transition metal modification. *J. Hazard. Mater.* **465**, 133231–133231. https://doi.org/10.1016/j.jhazmat.2023.133231 (2023).
26. Battumur, N., Sergelenbaatar, N., Bold, T. & Byambajav, E. Cerium-promoted nickel catalysts supported on yttrium-doped γ-alumina for carbon dioxide methanation. *J. CO2 Utilization*. **68**, 102380. https://doi.org/10.1016/j.jcou.2022.102380 (2023).
27. Xiong, J. et al. Production of bio-oil from waste cooking oil via microwave-assisted pyrolysis in the presence of waste eggshell CaO and HZSM-5: Process optimization and catalyst lifetime exploration. *Energy* **283**, 128416. https://doi.org/10.1016/j.energy.2023.128416 (2023).

28. Hakim, K. A. K. M., Tan, E. S., Habib, S. H., Hafriz, R. S. R. M. & Salmiaton, A. Investigation of waste-derived and low-cost calcium oxide-based catalysts in co-pyrolysis of EFB-HDPE to produce high quality bio-oil. *J. Anal. Appl. Pyrol.* **177**, 106375. https://doi.org/10.1016/j.jaap.2024.106375 (2024).
29. Evdokimenko, N. D., Kapustin, G. I., Tkachenko, O. P., Kalmykov, K. B. & Kustov, A. L. Zn Doping Effect on the Performance of Fe-Based Catalysts for the Hydrogenation of CO2 to Light Hydrocarbons. *Molecules (Basel Switzerland)*. **27** (3), 1065. https://doi.org/10.3390/molecules27031065 (2022).
30. Nagarajan, C., Annie Sujatha, R., Mani Rahulan, K., Little, A. & Vinitha, G. Optical nonlinearities of centrosymmetric pure and cerium doped calcium tungstate dumbbell shaped nanoparticles. *Opt. Mater.* **110**, 110512–110512. https://doi.org/10.1016/j.optmat.2020.110512 (2020).
31. Zheng, Y. et al. Catalytic activation of peroxodisulfate using shape-controlled cerium-manganese composite oxide for phenol degradation: Kinetics and degradation pathway investigation. *J. Rare Earths*. **42** (8), 1514–1523. https://doi.org/10.1016/j.jre.2023.10.008 (2023).
32. Lazzarini, A. et al. Nickel- and/or iron-based ceria-supported catalysts for CO oxidation in combustion exhaust gases. *J. Catal.* **430**, 115323. https://doi.org/10.1016/j.jcat.2024.115323 (2024).
33. Zhang, Y. et al. Intrinsic promotion mechanism of calcium oxide on ketone production during catalytic fast pyrolysis of biomass via experiment and density functional theory simulation. *Bioresour. Technol.* **410**, 131310–131310. https://doi.org/10.1016/j.biortech.2024.131310 (2024).
34. Ahmad, M. A. & Al-Maari, M. A. in, A. T. M., Hassan, H., & Alsobaai, A. M. Co-pyrolysis of oil palm empty fruit bunch and oil palm frond with low-density polyethylene and polypropylene for bio-oil production. Arabian Journal of Chemistry, 14(8), 103282. (2021). https://doi.org/10.1016/j.arabjc.2021.103282
35. Bhushan, D., Hooda, S. & Mondal, P. Co-pyrolysis of biomass and plastic wastes and application of machine learning for modelling of the process: A comprehensive review. *J. Energy Inst.*, 101973–101973 (2025).
36. Chang, S. H. An overview of empty fruit bunches from oil palm as feedstock for bio-oil production. *Biomass Bioenerg.* **62**, 174–181. https://doi.org/10.1016/j.biombioe.2014.01.002 (2014).

Figures

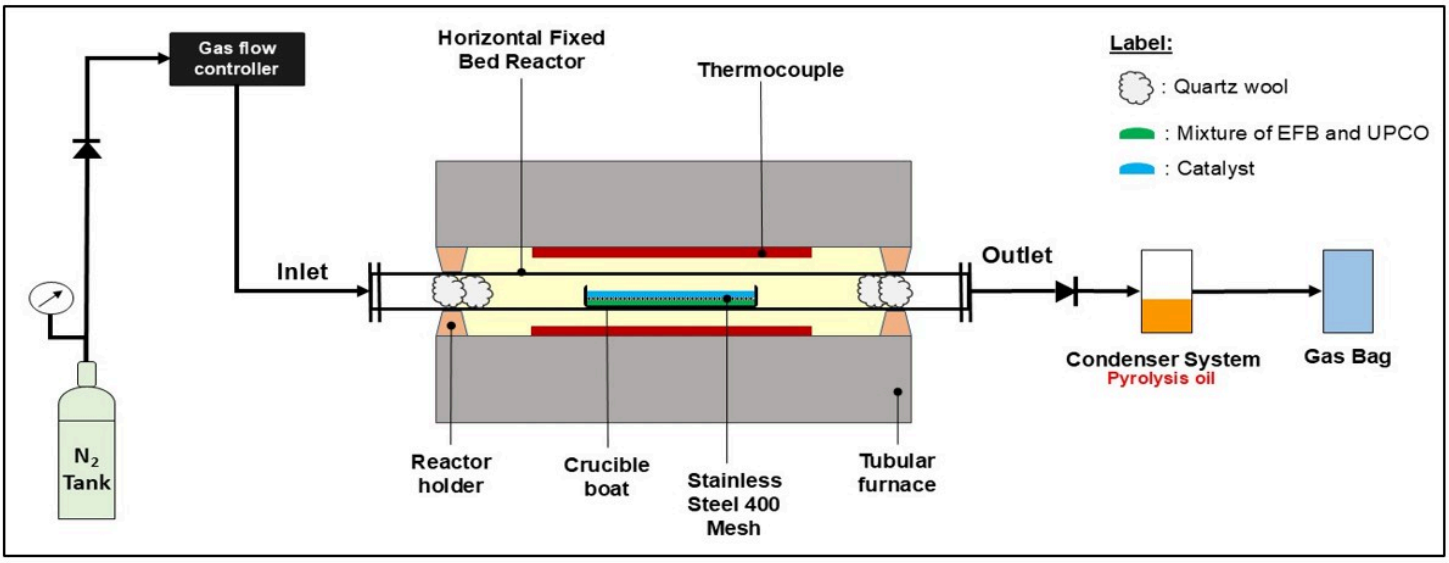


Figure 1

Figure 2.1 Schematic diagram pyrolysis setup

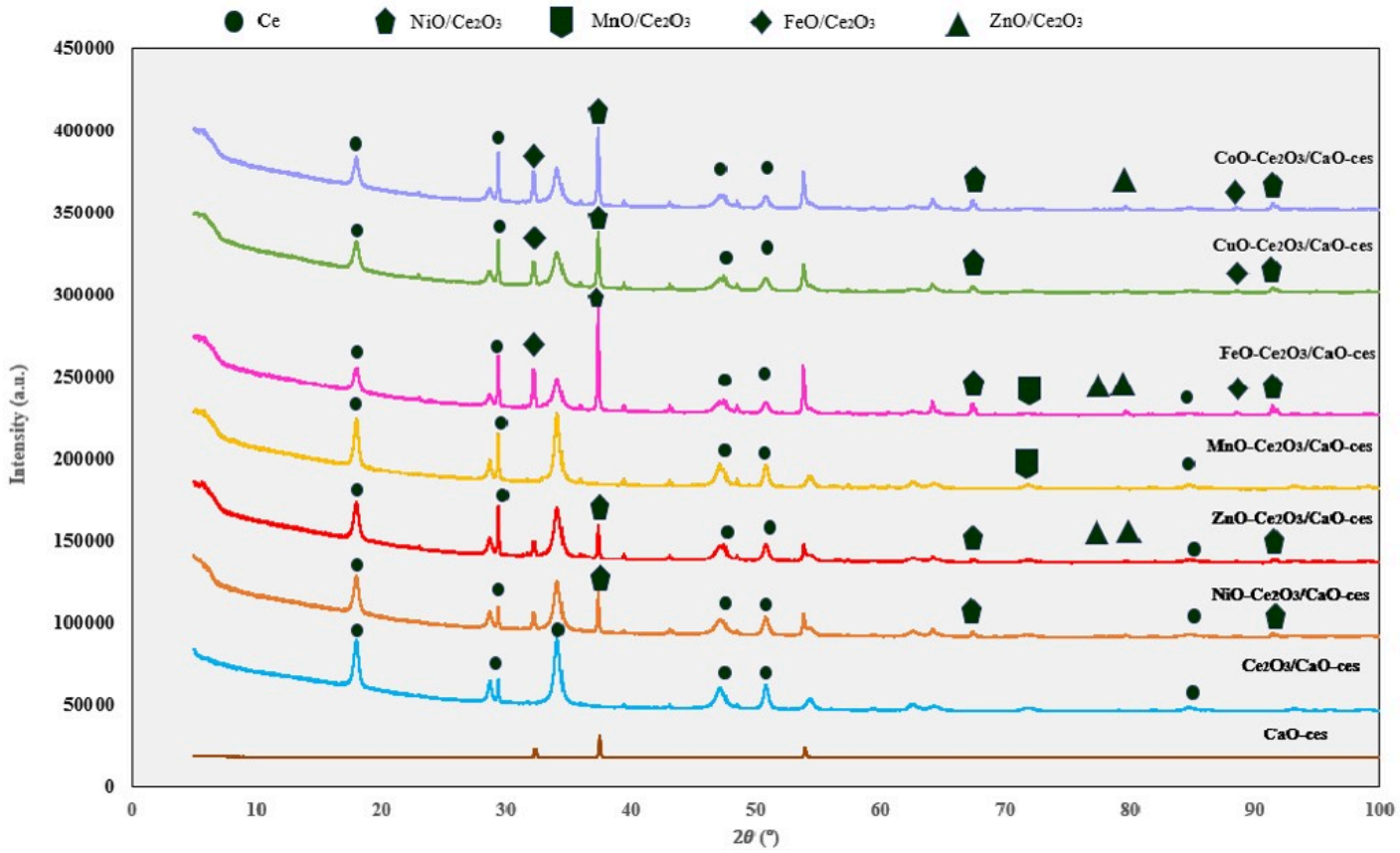


Figure 3

Figure 3.1 XRD Patterns of CaO-ces and metallic modified CaO-ces

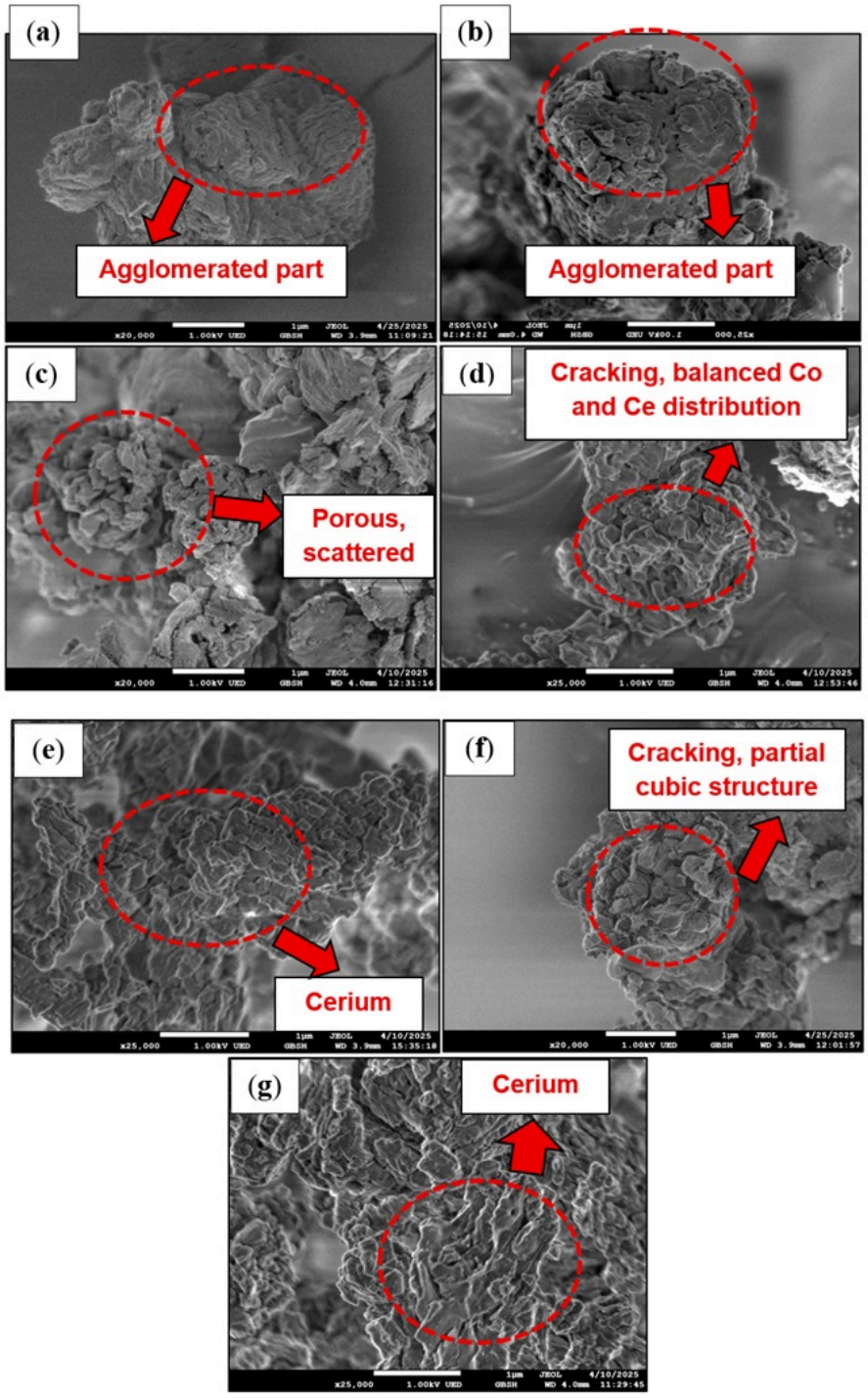


Figure 3

Figure3.2 FESEM Surface morphology for (a) Ce/CaO-ces, (b) Ni-Ce/CaO-ces, (c) Zn-Ce/CaO-ces, (d) Co-Ce/CaO-ces, (e) Fe-Ce/CaO-ces, (f) Cu-Ce/CaO-ces, (g) Mn-Ce/CaO-ces

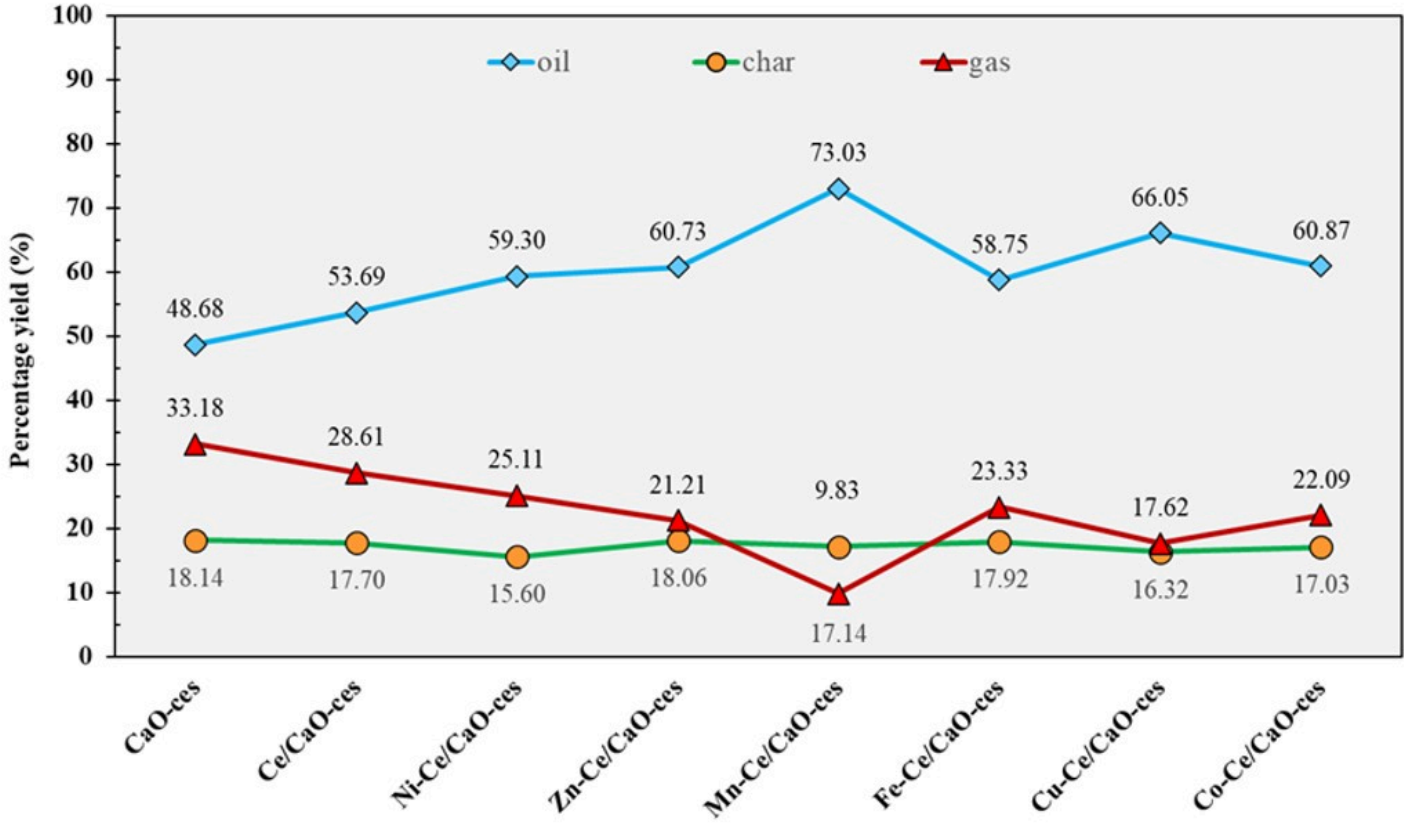


Figure 4

Figure 3.3 Composition of bio-oil, char and gas produced through catalytic pyrolysis using metallic modified CaO-ces.

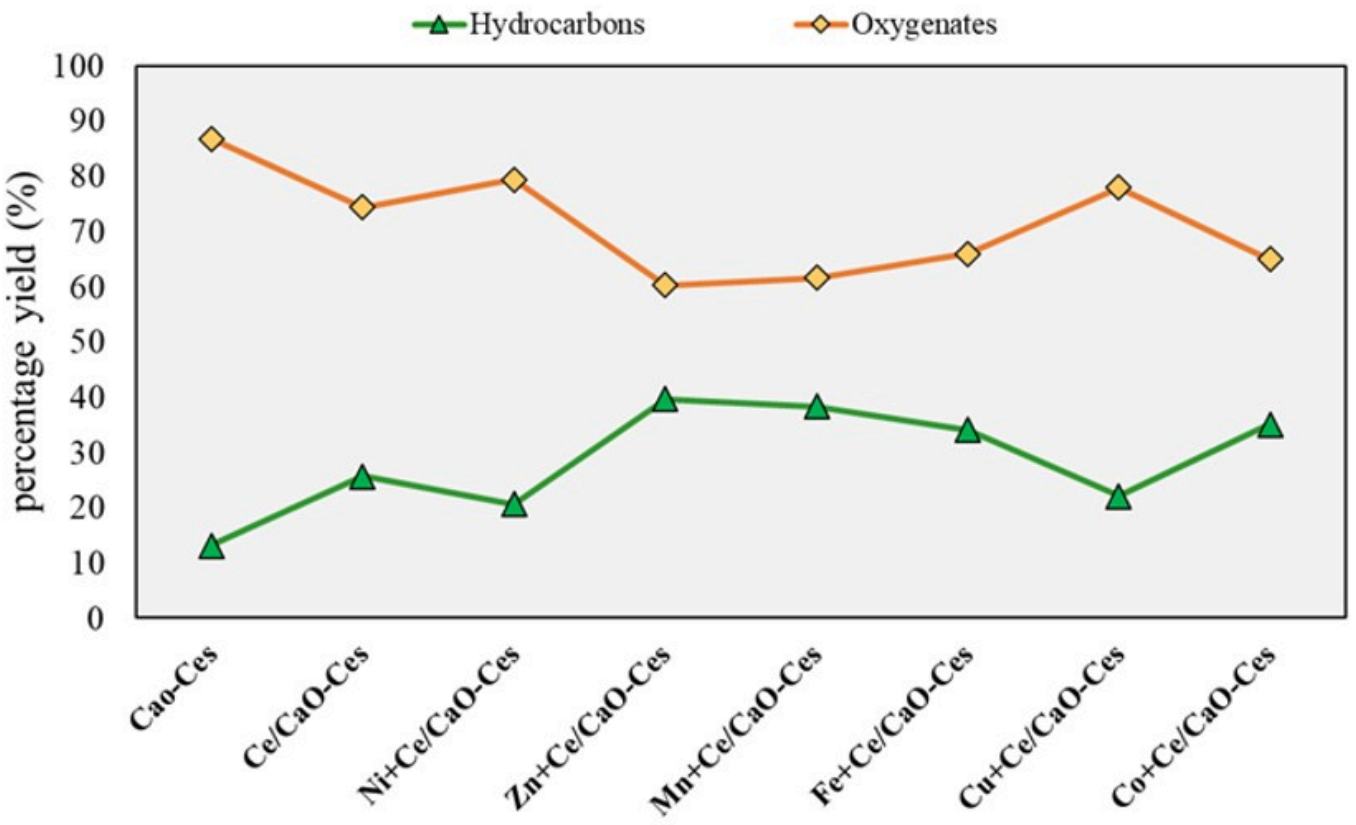


Figure 5

Figure 3.4 Percentage yield on hydrocarbons and oxygenates using different catalysts in line chart.